Smart Mater. Struct. **21** (2012) 075026 (17pp) doi:10.1088/0964-1726/21/7/075026

Advanced damper with negative structural stiffness elements

Liang Dong and Roderic S Lakes

Materials Science Program, University of Wisconsin-Madison, Madison, WI 53706, USA
and
Engineering Physics, University of Wisconsin-Madison, Madison, WI 53706, USA

E-mail: lakes@engr.wisc.edu

Received 27 November 2011, in final form 27 April 2012
Published 22 June 2012
Online at stacks.iop.org/SMS/21/075026

Abstract
Negative stiffness is understood as the occurrence of a force in the same direction as the imposed deformation. Structures and composites with negative stiffness elements enable a large amplification in damping. It is shown in this work, using an experimental approach, that when a flexible flat-ends column is aligned in a post-buckled condition, a negative structural stiffness and large hysteresis (i.e., high damping) can be achieved provided the ends of the column undergo tilting from flat to edge contact. Stable axial dampers with initial modulus equivalent to that of the parent material and with enhanced damping were designed and built using constrained negative stiffness effects entailed by post-buckled press-fit flat-ends columns. Effective damping of approximately 1 and an effective stiffness–damping product of approximately 1.3 GPa were achieved in such stable axial dampers consisting of PMMA columns. This is a considerable improvement for this figure of merit (i.e., the stiffness–damping product), which generally cannot exceed 0.6 GPa for currently used damping layers.

(Some figures may appear in colour only in the online journal)

1. Introduction

Energy absorption by mechanical damping ($\tan\delta$, with δ as the phase angle between stress and strain sinusoids) is of vital importance as one can damp vibrations in mechanical systems so as to prolong the service life of components. Damping of structures can be achieved via layers of high-damping materials, typically polymers, by external lumped dampers that may contain a viscous device, or using materials with intrinsically high damping. The reason is that structural metals such as steel, brass and aluminum alloys exhibit very low damping of 10^{-3} or less (e.g., steel: 0.0005; brass: 9×10^{-5}; aluminum alloy: $<10^{-5}$). A maximal combination of stiffness and damping is desirable for the damping layer and structural damping applications in which it is intended that vibration in machinery and vehicles be reduced. In structures, this is the product of structural stiffness or spring constant and damping; in materials, it is the product $|E^*|\tan\delta$, with $|E^*|$ being the absolute value of the complex Young's modulus (E^*). Figure 1 shows the stiffness–damping map for several classes of material at ambient temperature. The diagonal line in figure 1 represents $|E^*|\tan\delta = 0.6$ GPa. Most materials occupy the region to the left of that line. Structural materials occupy positions to the left or far to the left in the diagram, i.e., high stiffness but low damping. The $|E^*|\tan\delta$ product for structural metals are, for example, 0.1 GPa, 0.01 GPa and less than 0.001 GPa for steel, brass and aluminum alloy, respectively. Rubbery materials occupy the lower right, i.e., high damping but low stiffness (the $|E^*|\tan\delta$ product is less than 0.003 GPa). Materials that simultaneously combine high damping and high stiffness are not common. The region to the right of that line (i.e., $|E^*|\tan\delta > 0.6$ GPa) is favorable for vibration damping applications. Polymeric damping layers exhibit a peak value in damping from 0.1 to 1 or more, therefore polymer layers are commonly used to add damping to structural members. However, the product $|E^*|\tan\delta$ generally does not exceed 0.6 GPa in such materials either; even that value can be attained only over a narrow range of temperatures near the glass transition region [2]. In addition, damping layers work best for objects subjected

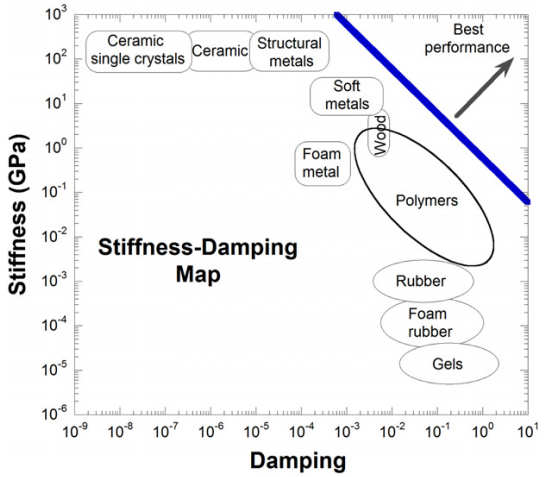

Figure 1. Stiffness–damping map for several classes of materials at ambient temperature. The diagonal line (i.e., the blue line) represents $|E^*| \tan \delta = 0.6$ GPa. Adapted from Lakes [1].

to bending due to distance from the neutral axis; for axial deformation, they are not as effective [3]. Therefore superior structures and materials are of interest. In that vein, negative stiffness is being considered.

Composite theory predicts that damping of heterogeneous structures or composites containing a constituent of negative stiffness can far exceed all standard bounds by appropriate tuning of the negative stiffness phase [4]. Extreme damping is observed in structures containing buckled tubes [5]; these exhibit negative stiffness during post-buckling. Recent experimental measurements by Lakes and co-workers [6, 7] confirmed that values of the composite Young's modulus and damping can far exceed all existing bounds, and in fact exhibited Young's modulus higher than that of any known material, even diamond.

Negative stiffness is a counterintuitive phenomenon that entails a reversal of the usual directional relationship between stress and strain in deformed objects. Negative stiffness can be achieved in a variety of ways, as follows. A slender bar in a post-buckled 'S' shaped configuration is in unstable equilibrium [8] unless it is constrained laterally. Such a bar can undergo a snap-through effect if pressed transversely near the center. A negative stiffness region can be measured experimentally provided the displacement, not the force, is controlled. One can easily verify the properties of such post-buckled bars with the aid of a flexible plastic ruler. Flexible thin tubes in the post-buckling regime exert a decreasing force with an increase in deformation, hence a negative stiffness. Flexible tetrakaidecahedra [9] exhibit a non-monotonic force–deformation relation, hence they exhibit negative stiffness over a range of strain. They were considered as models of single cells in foams and deformed in compression under displacement control. Such negative stiffness is not stable unless stabilized by a constraint on the deformation.

In this work, the post-buckling properties of PMMA (polymethyl methacrylate) columns with different end conditions were experimentally studied; stable modules composed of clamped and press-fit PMMA columns were then constructed. The stress–strain curves are obtained via a servohydraulic test machine. The effective modulus is similar to that of the parent material but with enhanced damping. Furthermore, it was found that with appropriate pre-strain, the effective damping of the damper module can attain values as high as approximately 1, and a maximum effective stiffness–damping product ($|E^*| \tan \delta$) of approximately 1.3 GPa was achieved, a significant improvement for this figure of merit.

2. Experimental details

In this work, commercial PMMA (extruded acrylic rod, McMaster-Carr, #8531K11) rods were used. The rationale is that PMMA is a structural polymer that has a moderate value of intrinsic damping and can support a fairly large strain. First, axial deformation and post-buckling hysteresis of columns was studied to support the design of lumped axial dampers. To that end, columns of nominal 3.175 mm (1/8″) diameter with different lengths of 100, 80, 60, 40, and 30 mm were cut with a low-speed diamond saw. The diameters of these columns were finally measured with a digital caliper to ensure accuracy; the true diameters of these columns vary from 3.1 to 3.3 mm (because there is a variation in diameter, the nominal diameter value is rounded to the nearest hundredth, i.e., 3.18 mm, is used throughout the entire paper). Both ends of these columns were then sanded and polished to ensure flat surfaces. Force–displacement relationship measurements were performed at room temperature using a servohydraulic (maximum force capacity 100 kN, MTS system Corp. Mpls, MN) test system under compression in displacement control with 1 Hz sinusoidal waveforms as the input. The AC amplitude of the displacement was controlled by setting 'Span' to a certain value, which corresponds to a certain fraction of the maximum displacement allowable by the control system. A sufficient 'Span' (i.e., a sufficient fraction of the maximum displacement allowable by the control system) enables post-buckling to occur during loading. Both the magnitude and the phase of the force and displacement were captured by a digital oscilloscope. As a comparison, PMMA columns of the same size (3.18 mm diameter, 60 mm length) but with a different end condition (point ends) were also tested.

Stable axial dampers were designed and built as proof of concept, taking advantage of the effects in post-buckling of press-fit flat-ends columns. The frame of the damper module is composed of two 50.8 mm (2″) diameter 6.35 mm (1/4″) thick PMMA (cast acrylic circle, McMaster-Carr, #1221T23) disks supported by two identical clamped dog-bone shaped PMMA rods between the two PMMA disks. Each dog-bone shaped PMMA rod is composed of three components: one 3.18 mm (1/8″) diameter PMMA column (length of 50 mm) with an effective length of 30 mm, clamped at both ends by two 6.35 mm (1/4″) diameter PMMA (extruded acrylic rod, McMaster-Carr, #8531K11) rods by feeding it into blind holes (3.18 mm diameter and 10 mm depth) drilled in the

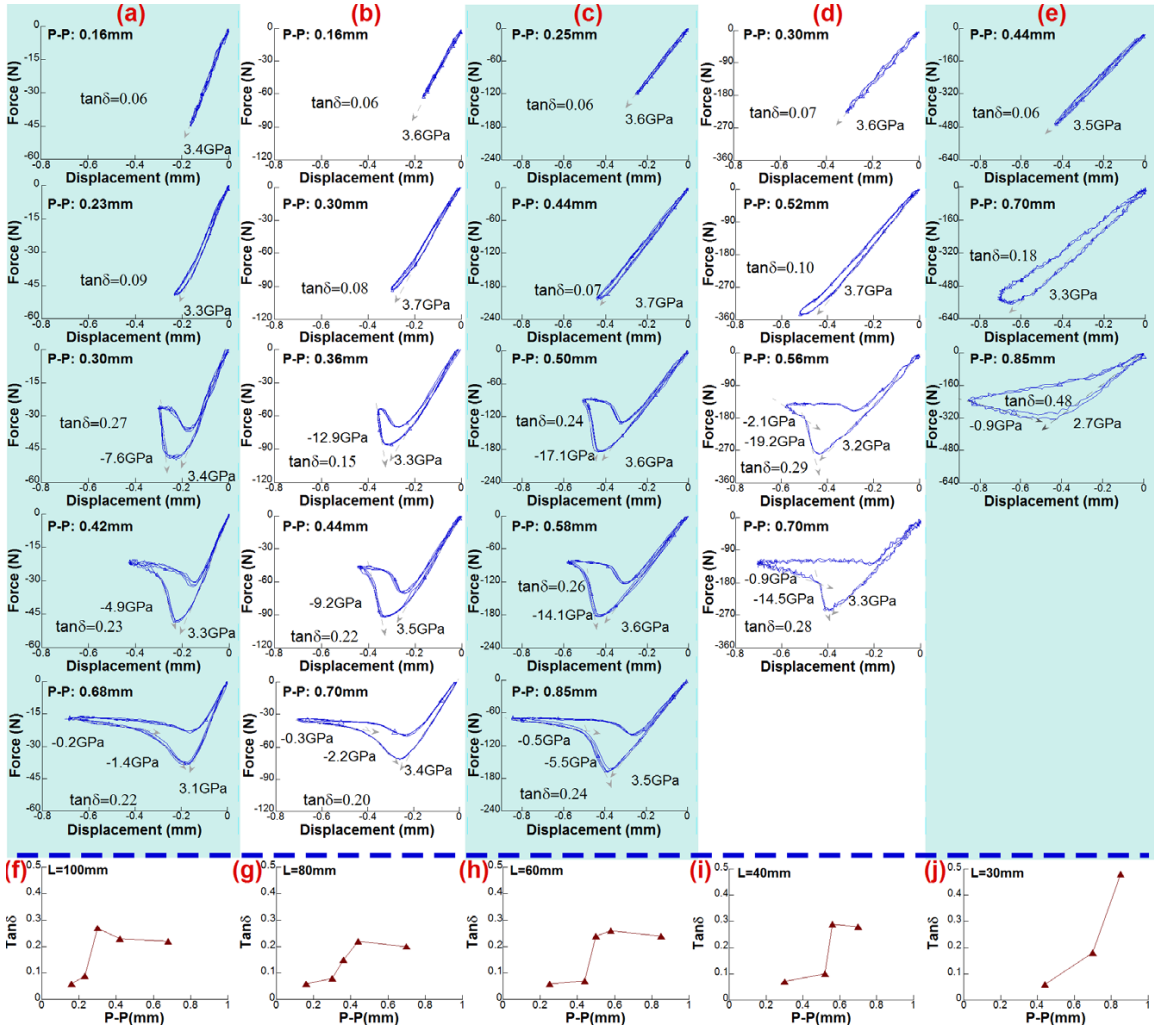

Figure 2. Force–displacement relationship of press-contact flat-ends PMMA columns of 3.18 mm diameter and various lengths under 1 Hz compression tests at various peak-to-peak excursions (P–P) in displacement. The flat ends are allowed to tilt at the edges. Each column of the figure (vertical array of images from (a) to (e)) represents the behaviors of a testing specimen with a specific length ((a) 100 mm; (b) 80 mm; (c) 60 mm; (d) 40 mm; (e) 30 mm). Damping as a function of peak-to-peak excursion (P–P) in displacement for each testing specimen is summarized in (f)–(j).

6.35 mm (1/4″) diameter PMMA rods. The 6.35 mm (1/4″) diameter PMMA rods (length of 18 mm) with effective length of 15 mm were also clamped by feeding them into blind holes (6.35 mm diameter and 3 mm depth) drilled in the PMMA disks. 3.18 mm (1/8″) diameter 60 mm length flat-ends PMMA columns were press-fitted in between the two PMMA disks. The force–displacement relationship was measured by the servohydraulic testing system under displacement control during 1 Hz compression tests. To tune the effective stiffness of the press-contact 3.18 mm (1/8″) diameter 60 mm length columns, the DC component of the displacement was varied in order to provide pre-strain.

Damping ($\tan\delta$) is proportional to the area that is enclosed by the Lissajous figure (i.e., the closed curve of force versus displacement sinusoids; when the input displacement is sinusoidal, the output force is sinusoidal with the same frequency, but it has a different phase shift δ with respect to the input displacement. Using an oscilloscope capable of plotting one signal against another, the force output versus displacement input produces a Lissajous figure enclosed by force–displacement rectangular boundaries. The rotation direction of the Lissajous figure is clockwise). It is easy to determine the damping capacity when the Lissajous figure is an ellipse, as it is for linear systems or materials; $\tan\delta$ equals the ratio of the width of the elliptic Lissajous figure to the length of the projection of this elliptic Lissajous figure onto the displacement axis [10]. When the Lissajous figure exhibits nonlinearity, the damping capacity can be obtained by referring the area ratio of this nonlinear Lissajous figure to an elliptic Lissajous figure with a known phase lag (e.g.,

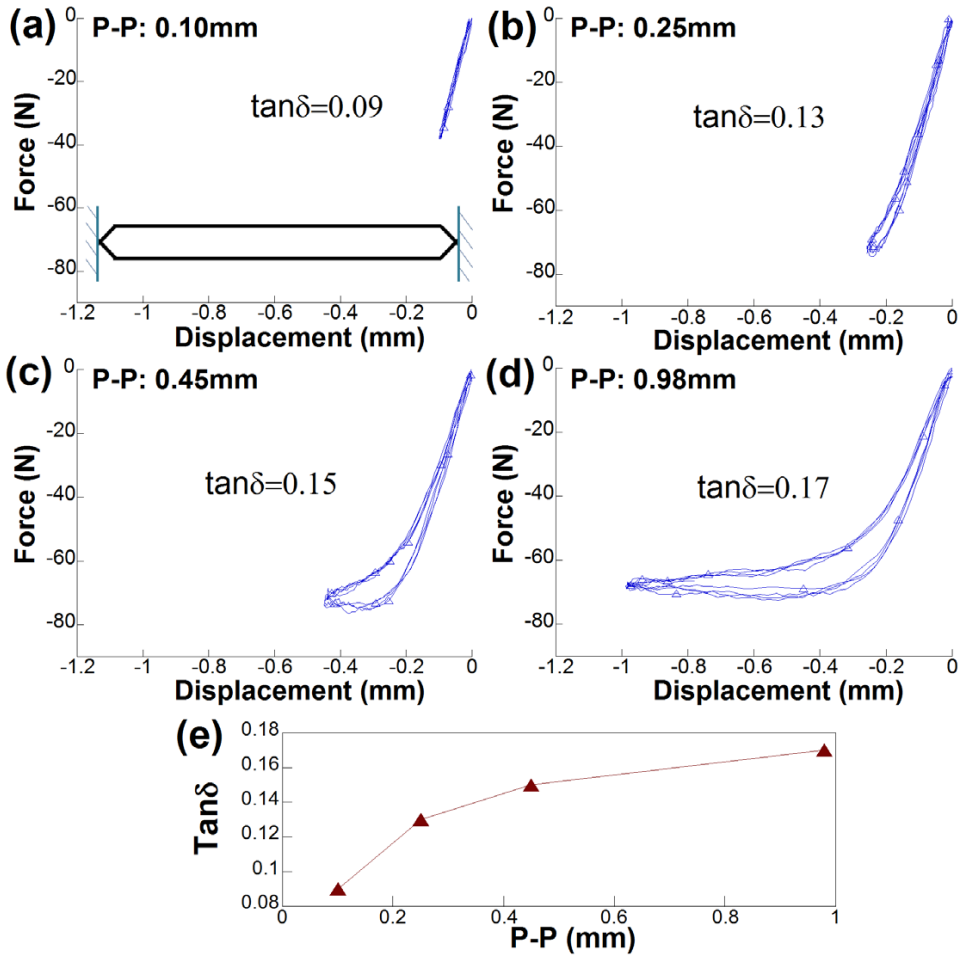

Figure 3. Force–displacement relationship of a press-contact point-ends PMMA column ($L = 60$ mm; diameter $= 3.18$ mm) under 1 Hz compression tests. Inset shows the sketch of the point-ends PMMA column. Damping as a function of peak-to-peak excursion (P–P) in displacement is summarized in (e).

$\delta = 1$ (rad.)) within the same force–displacement rectangular boundaries [10]. Quantitative interpretation of the elliptic Lissajous figure can be found in [10]. The effective stiffness is determined by referring to the slope of the line passing through the initial loading point and dividing the area enclosed by the Lissajous figure in half. Engineering strain and stress were used in the present study.

3. Results and discussion

3.1. Force–displacement relationship of non-pre-strained PMMA columns with different end conditions in compression tests

Figures 2(a)–(e) shows the force–displacement relationship of press-contact flat-ends 3.18 mm diameter PMMA columns with different lengths ((a) 100 mm, (b) 80 mm, (c) 60 mm, (d) 40 mm and (e) 30 mm) under 1 Hz compression tests at various AC amplitudes in displacement. Each vertical array of images from (a) to (e) represents the behaviors of a press-contact flat-ends PMMA column (3.18 mm diameter) with a specific length. The peak-to-peak excursion (P–P) of the sinusoidal displacement input is given as an inset to each figure. The flat ends of these columns have press contact and are allowed to tilt at the edges under compression loading. The slope of the tangent line for each segment on the loading portion (in which displacement keeps increasing) of the Lissajous figure is shown, which indicates the Young's modulus at that specific stage during loading. The loading and unloading paths on a nonlinear Lissajous figure are shown in figure 5(b).

The Young's modulus ($|E^*|$) of these PMMA columns is about 3.5 GPa within the linear viscoelastic region (i.e., when the Lissajous figure is an elliptic). The Lissajous figure changes from a narrow elliptic to a curled shape when increasing the AC amplitude of the displacement as the end condition changes from flat to edge contact. A negative slope, which indicates a negative stiffness on part of the force–displacement curve, is observed when the end condition changes due to tilt of the ends during post-buckling (line art figures illustrating flat-end buckling and end-tilt

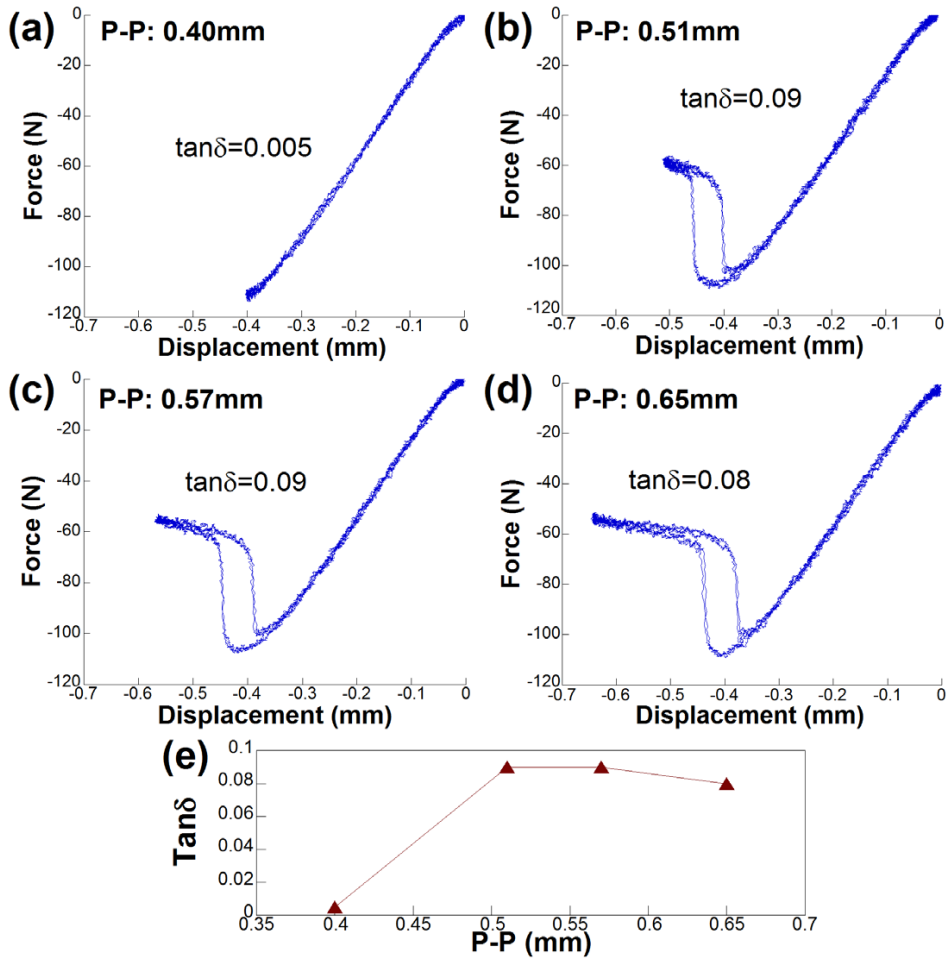

Figure 4. Force–displacement relationship of press-contact flat-ends polycarbonate column ($L = 60$ mm; diameter $= 3.18$ mm) under 1 Hz compression tests. The intrinsic damping (0.005) of polycarbonate was determined via BVS. Damping as a function of peak-to-peak excursion (P–P) in displacement is summarized in (e).

buckling are shown in figure 5(b)). The effective contact area being used to calculate the modulus within the nonlinear region of the Lissajous figure is still the cross-sectional area of the column, as this is the most general way to express modulus. The strain for onset of buckling increases with increasing diameter to length ratio of the column. The buckling enhanced the damping significantly from the intrinsic value about 0.07 to about 0.2, or even higher, by introducing an extra region partially enclosed by these negative slope lines on the Lissajous figure. Damping as a function of peak-to-peak excursion (P–P) in displacement for each flat-ends PMMA column being studied is summarized in figures 1(f)–(j). Damping first increases with increasing buckling until reaching a peak value, and then decreases with further post-buckling. Damping caused by the post-buckling effect is higher in columns with smaller diameter to length ratios, but is limited to the amount of deformation by the compression yield strain. The critical point for the onset of the end condition changing from flat surface to edge contact shifts to lower strain after multiple loading cycles, and this is attributed to the plastic indentation at the edges due to stress concentration. This phenomenon can be minimized by end caps or by using materials with high wear resistance.

To evaluate the contribution of the end condition to the post-buckled region on the Lissajous figure, the force–displacement relationship of point-ends columns has also been tested. Figure 3 shows the behaviors of a point-ends PMMA column (60 mm length and 3.18 mm diameter). The Lissajous figure also becomes nonlinear when the column begins to buckle, but the post-buckling region does not give as negative a slope as the flat-ends columns do. Also, the damping capacity is not as high as the flat-ends column can attain when the end condition changes from flat to edge contact. It is thus concluded that the greatly enhanced damping and negative stiffness are attributed to the changing of the end conditions from flat surface to edge contact.

The mechanical property entailed by post-buckling of press-contact flat-ends columns can be utilized to design

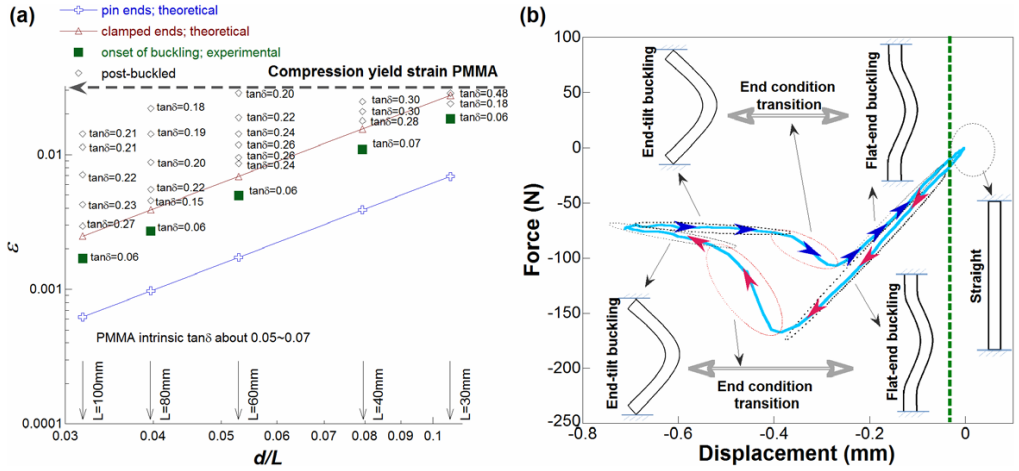

Figure 5. (a) Summary of press-contact flat-ends PMMA column buckling: damping, strain versus aspect ratio d/L. The critical strain for losing stability for press-contact flat-ends column is between theoretical values for pin-ends and clamped-ends columns. (b) Example of a nonlinear Lissajous figure (press-contact flat-ends PMMA column of 3.18 mm in diameter and 60 mm in length under 1 Hz compression test; peak-to-peak excursion (P–P) in displacement is 0.72 mm) to illustrate how the end conditions change during the loading history (the line art figures are exaggerated). The arrows on the Lissajous figure represent the rotation direction of the Lissajous figure. The dashed lines represent the onset of elastic buckling.

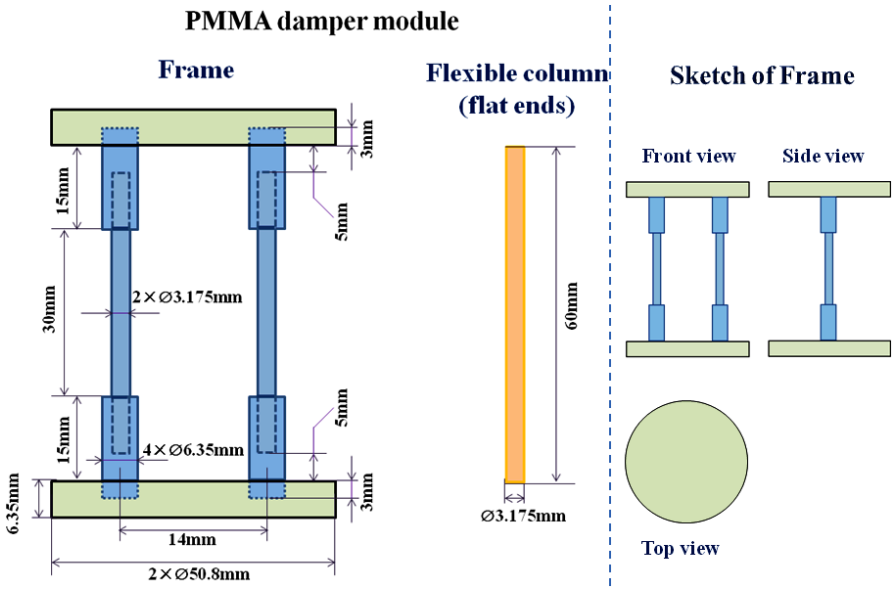

Figure 6. Sketch of PMMA axial damper module. The damper module is composed of a frame and one or more press-fit flat-ends column(s). The frame is supported by two dog-bone support rods clamped in the bases (i.e., the disks).

advanced axial dampers. In the following, flat-ends PMMA columns have been used as the components to improve the damping of the system being studied.

3.2. Generic application of end-tilt column buckling for damping improvement

The method for damping enhancement via end-tilt column buckling has general applications, and is not restricted to specific materials. For example, polycarbonate, a widely used thermoplastic polymer, has a high impact resistance and high glass transition temperature (∼150 °C). It can undergo a large plastic deformation without cracking or breaking. However, low intrinsic damping (about 0.005–0.008 [11, 12]) is a crucial issue of this material. It has been shown that, by virtue of end-tilt column buckling, the damping capacity of the polycarbonate (Mcmaster-Carr, #8571K11) can be improved considerably. The intrinsic damping of polycarbonate was measured via broadband viscoelastic

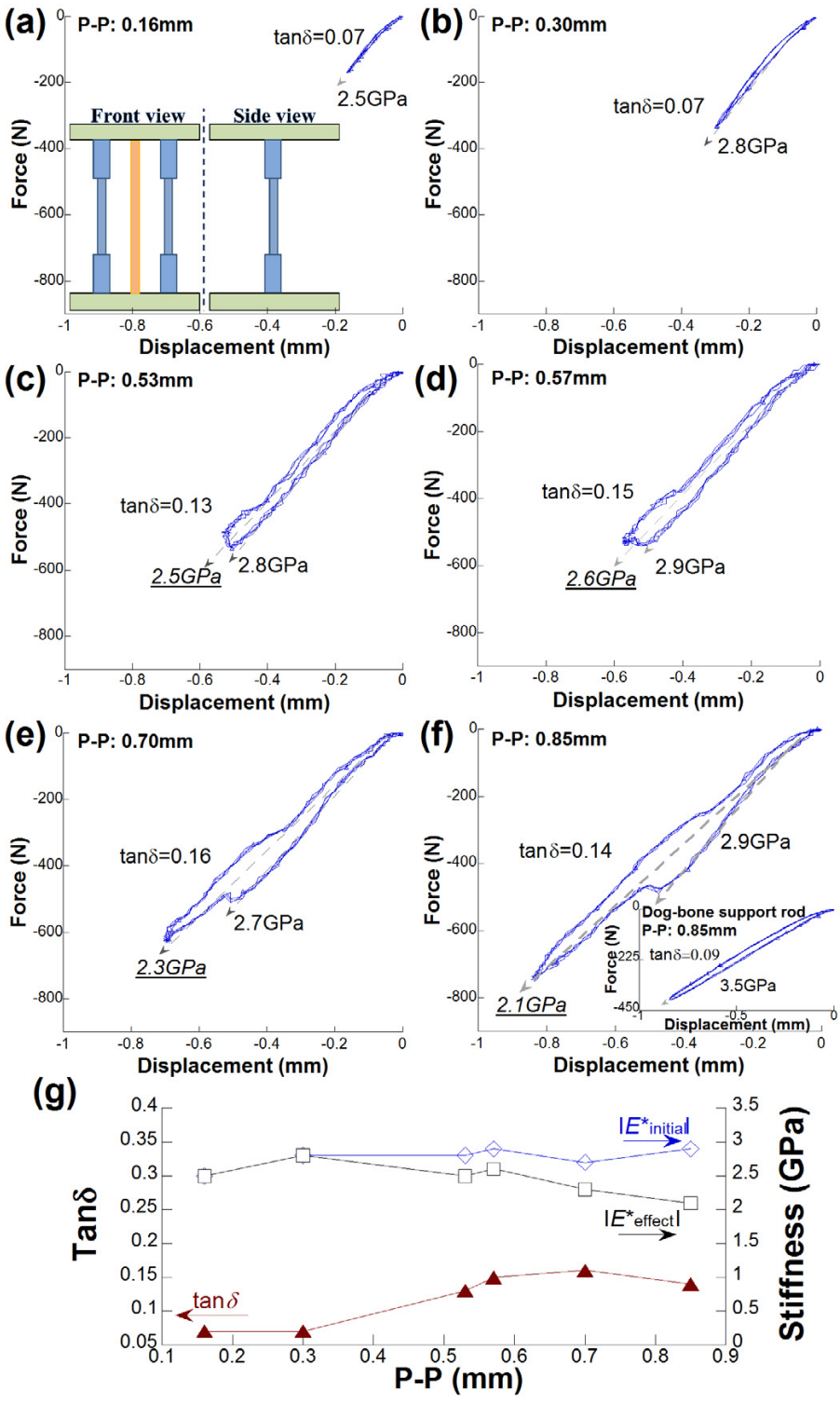

Figure 7. Force–displacement relationship of a non-pre-strained PMMA axial damper module with one press-fit flat-ends PMMA column ($L = 60$ mm; diameter $= 3.18$ mm) under 1 Hz compression tests. Insets show the sketch of this module and the force–displacement relationship of the non-pre-strained dog-bone support rod under 1 Hz compression tests with a peak-to-peak excursion (P–P) of 0.85 mm in displacement. Damping, initial stiffness, and effective stiffness of the module as a function of peak-to-peak excursion (P–P) in displacement are summarized in (g).

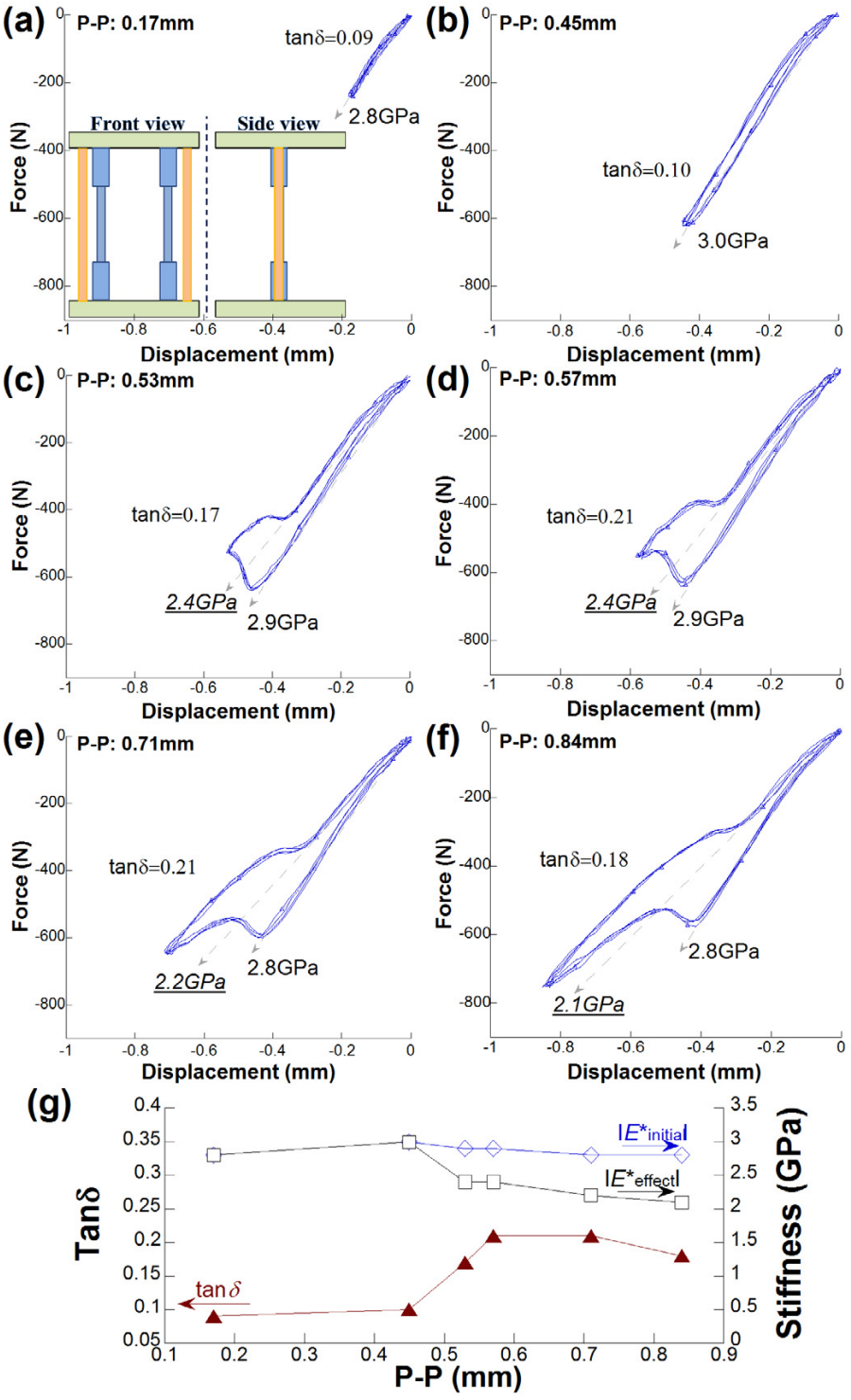

Figure 8. Force–displacement relationship of a non-pre-strained PMMA axial damper module with two press-fit flat-ends PMMA columns ($L = 60$ mm; diameter $= 3.18$ mm) under 1 Hz compression tests. Insets show the sketch of this module. Damping, initial stiffness, and effective stiffness of the module as a function of peak-to-peak excursion (P–P) in displacement are summarized in (g).

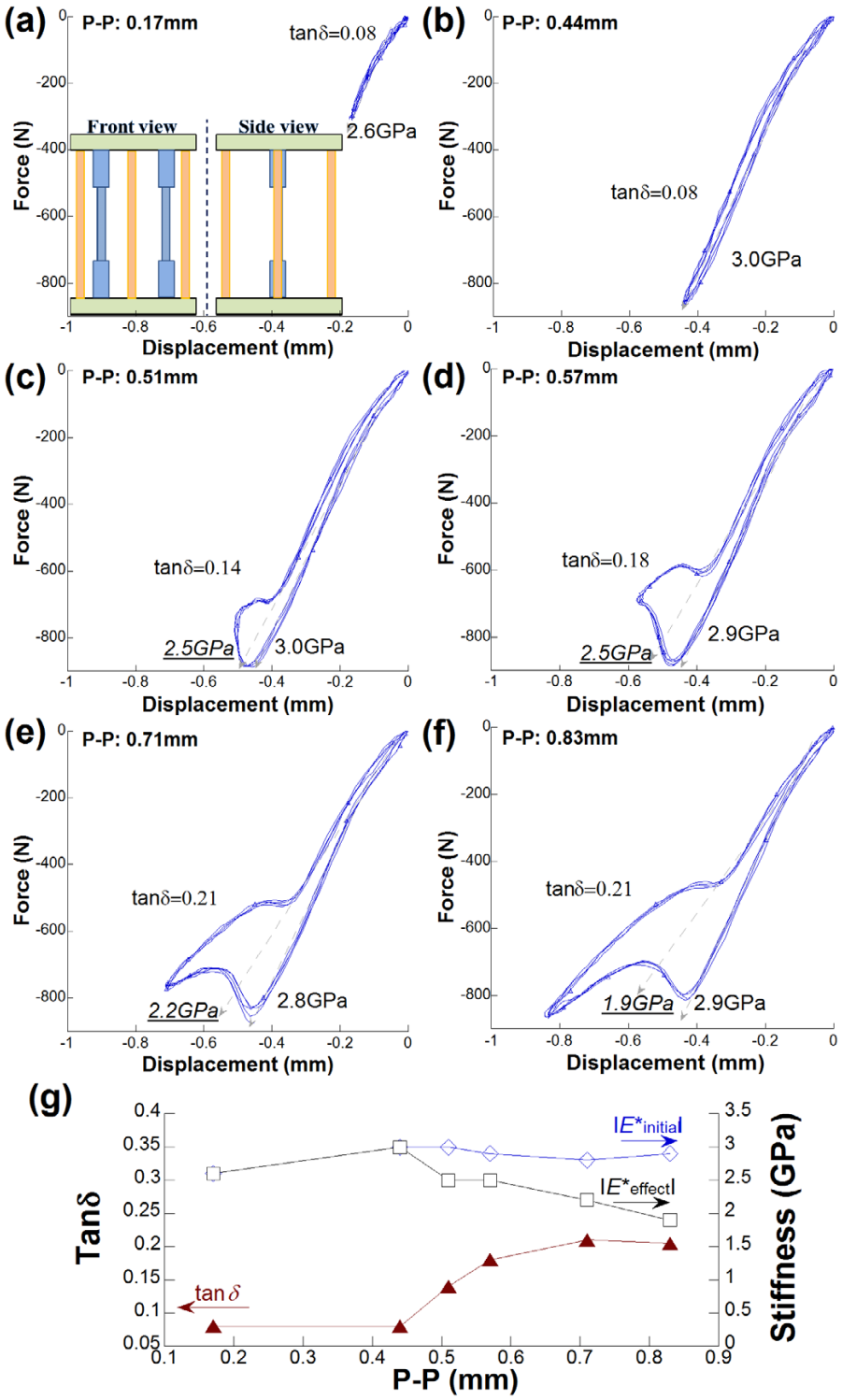

Figure 9. Force–displacement relationship of a non-pre-strained PMMA axial damper module with four press-fit flat-ends PMMA columns ($L = 60$ mm; diameter $= 3.18$ mm) under 1 Hz compression tests. Insets show the sketch of this module. Damping, initial stiffness, and effective stiffness of the module as a function of peak-to-peak excursion (P–P) in displacement are summarized in (g).

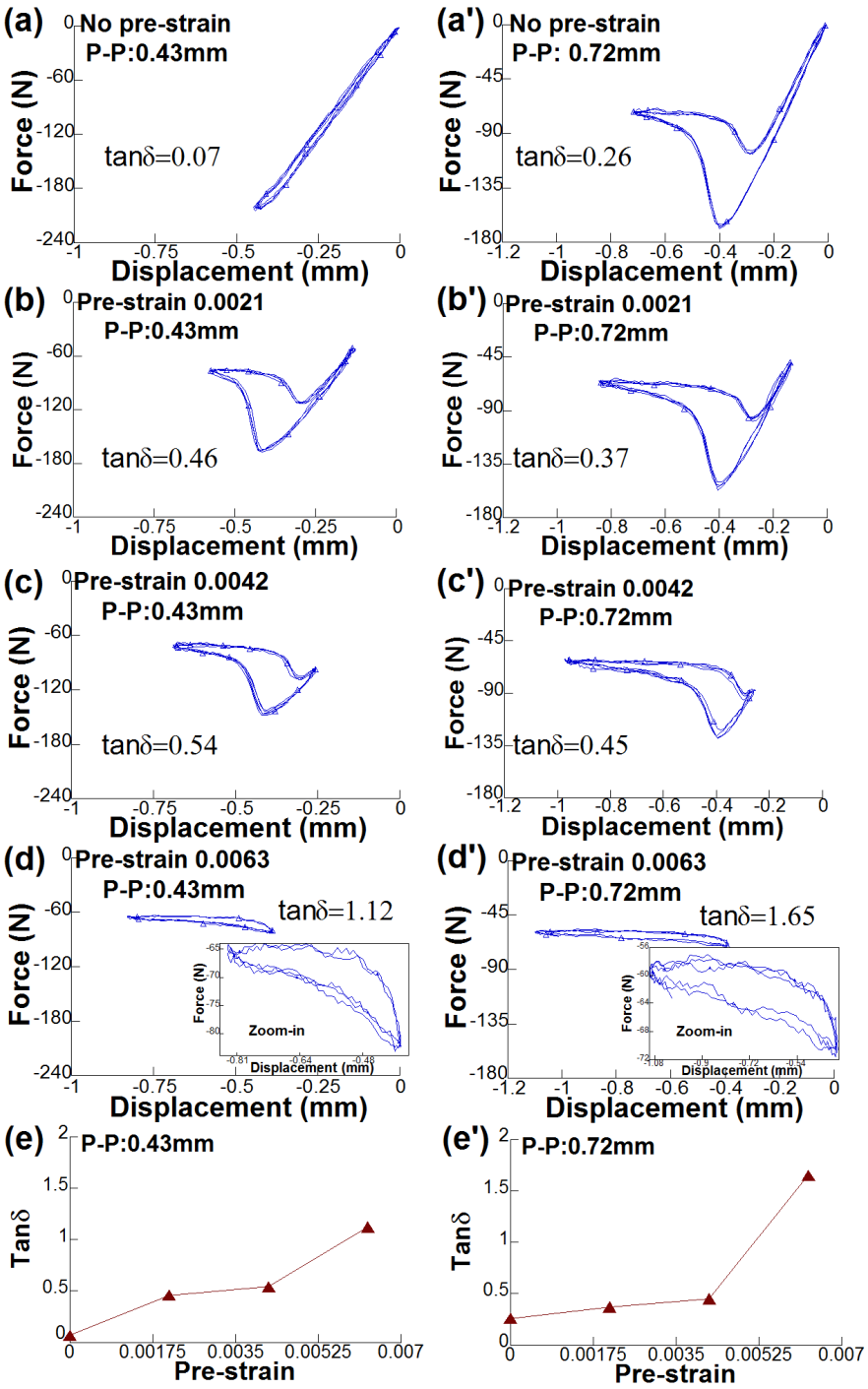

Figure 10. Force–displacement relationship of a press-contact flat-ends PMMA column ($L = 60$ mm; diameter $= 3.18$ mm) with different pre-strains. Insets show the Lissajous figures at a reduced scale. Damping versus pre-strain is summarized for fixed peak-to-peak excursion (P–P) in displacement: (e) P–P: 0.43 mm and (e′) P–P: 0.72 mm.

spectroscopy (BVS) [13], a technique with the capability of accurately measuring damping as low as 0.001. This was necessary because the phase resolution of the servohydraulic test frame is about 0.01. The measured intrinsic damping of polycarbonate is about 0.005 at 1 Hz, and is consistent with published results [11, 12]. Damping increases from the intrinsic value to about 0.09 for a flat-ends polycarbonate column of 3.18 mm diameter and 60 mm length when it

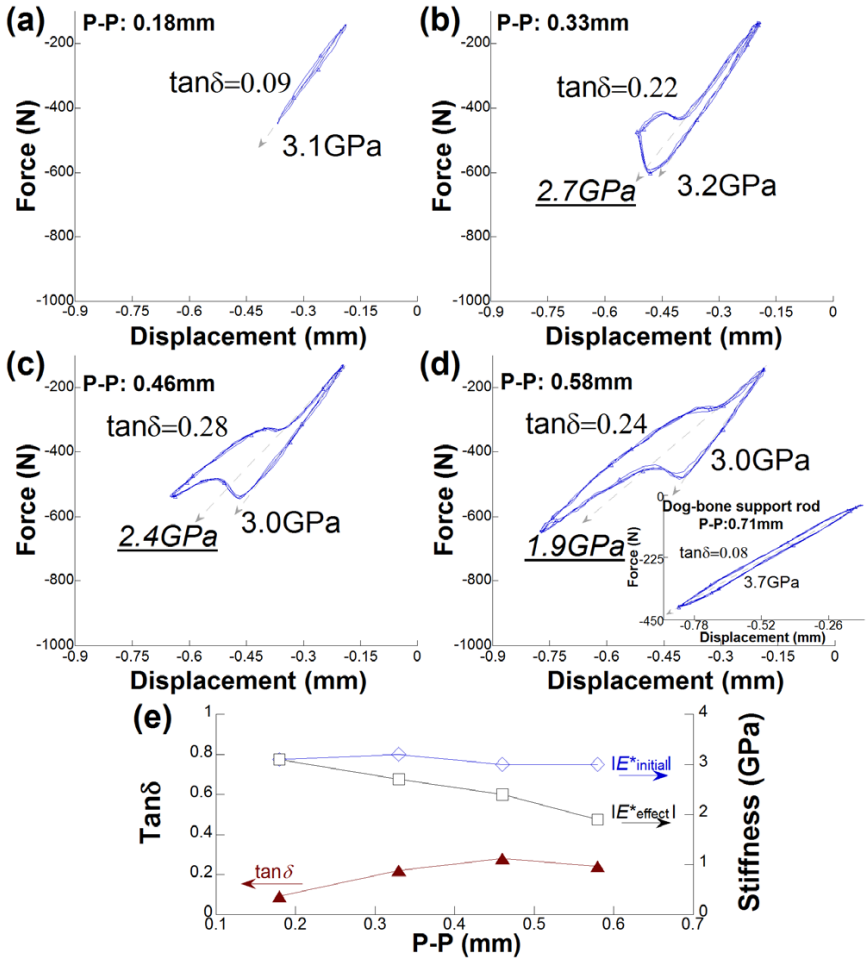

Figure 11. Force–displacement relationship of a PMMA axial damper module with two press-fit flat-ends PMMA columns ($L = 60$ mm; diameter $= 3.18$ mm) under 1 Hz compression tests with a pre-strain of 0.0023 for the press-fit columns. Insets show the force–displacement relationship of the dog-bone support rod (with the same pre-deformation) under 1 Hz compression tests with a peak-to-peak excursion (P–P) in displacement of 0.71 mm. Damping, initial stiffness, and effective stiffness of the module as a function of peak-to-peak excursion (P–P) in displacement are summarized in (e).

has post-buckled (without pre-strain) (figure 4). The damping capacity of polycarbonate column via post-buckling is about eighteen times the intrinsic value, but is lower than PMMA columns under the same experimental conditions. This is considered as a result of the contribution of the intrinsic damping to the overall damping during buckling. However, low intrinsic damping is not necessarily a drawback if the columns are used with some pre-strain, as will be presented in a later section.

3.3. Design of axial damper module

Properties including damping capacities and effective strain versus diameter to length ratio of non-pre-strained flat-ends PMMA columns in compression tests are summarized in figure 5(a) based on figure 1. The theoretical strains for losing stability of columns with pin-ends and clamped-ends conditions according to the Euler column buckling equations are given for comparison with the experimental strains for the onset of buckling of press-contact flat-ends columns. The Euler buckling equation [14] is expressed as follows: $\varepsilon = \pi^2 I/[(KL)^2 A]$, where ε, I, K, L and A represent the theoretical strain for losing stability, area moment of inertia, effective length factor, length of column, and cross sectional area of the column, respectively. For columns with pin ends, $K = 1$; for columns with clamped ends, $K = 0.5$.

As described in section 3.2, the stable PMMA axial damper modules are supported by two clamped dog-bone shaped PMMA rods (figure 6). The effective length of the middle part of the dog-bone support rod is 30 mm, with a diameter of 3.18 mm, and the onset strain for losing stability of this segment is about 0.0276 according to the Euler column buckling equation. So this supporting portion of the structure will be stable when the press-fit columns buckle, as they

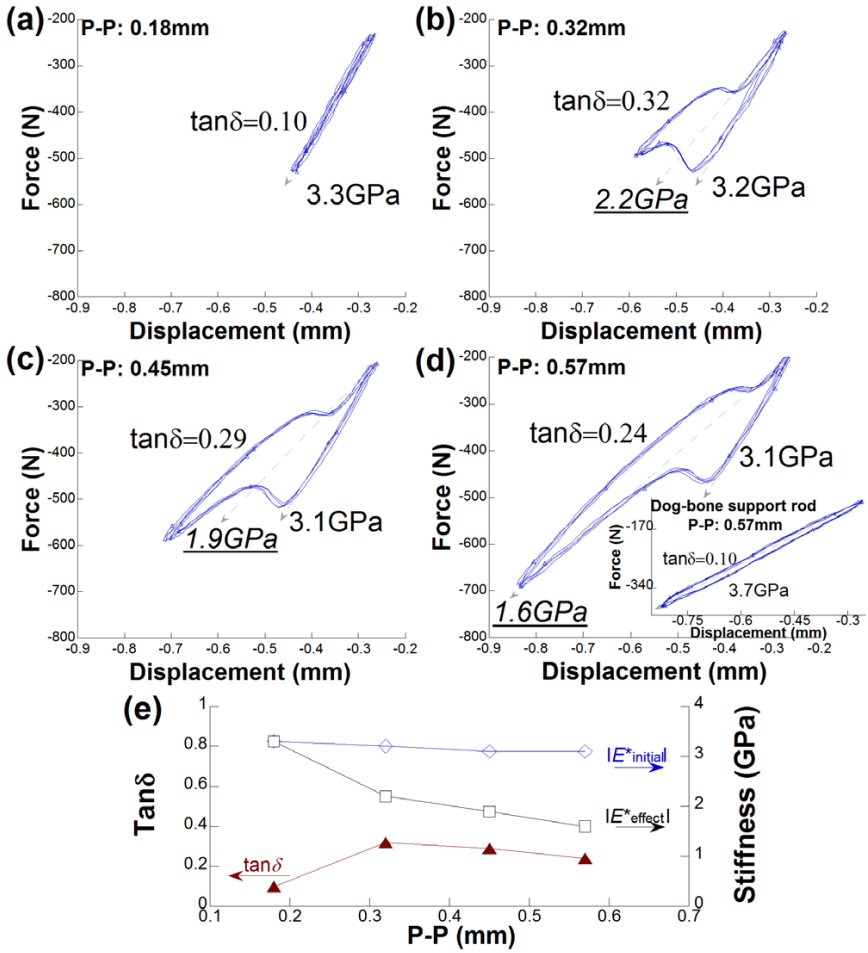

Figure 12. Force–displacement relationship of a PMMA axial damper module with two press-fit flat-ends PMMA columns ($L = 60$ mm; diameter $= 3.18$ mm) under 1 Hz compression tests with a pre-strain of 0.0036 for the press-fit columns. Insets show the force–displacement relationship of the dog-bone support rod (with the same pre-deformation) under 1 Hz compression tests with a peak-to-peak excursion (P–P) in displacement of 0.57 mm. Damping, initial stiffness, and effective stiffness of the module as a function of peak-to-peak excursion (P–P) in displacement are summarized in (e).

are designed to do. The effective cross-sectional area of the PMMA frame is calculated by referring to the Reuss composite model (the PMMA disks, i.e., the bases of the frame, are not being considered as a loading component in calculation, as the disks have the same function as the specimen mounting plates of the servohydraulic machine) as follows, $A_{\text{frame}} = 1/\{[L_1/(L_1 + 2L_2)]/A_1 + 2[L_2/(L_1 + 2L_2)]/A_2\}$, where L_1, A_1 and L_2, A_2 represent the length and cross-sectional area of the 3.18 mm diameter rod and 6.35 mm diameter rod, respectively. When press-fit flat-ends PMMA columns are incorporated, the effective cross-sectional area of the damper module is expressed as $A_{\text{effective}} = A_{\text{frame}} + nA_{\text{column}}$, where n and A_{column} represent the number of press-fit columns being used and the cross-sectional area of such a column.

Due to machining tolerances, the frame of the damper module needs to be pre-deformed by about 0.05 mm for the press-fit columns to have solid contact with the bases of the frame. In the following, the pre-strain refers to that of the press-fit column.

3.4. Force–displacement relationship of non-pre-strained damper module in compression tests

3.4.1. Damper module with one press-fit flat-ends PMMA column. Figure 7 presents the behaviors of a PMMA axial damper module with one press-fit 3.18 mm diameter 60 mm length flat-ends PMMA column under 1 Hz compression tests without pre-strain. The inset of figure 7(a) shows the sketch of this module. With increasing deformation, the damping capacity of the module increases by virtue of the buckling of the press-fit column, and the lumpy shape of the Lissajous figure is an indication of its buckling. The effective stiffness of the module is similar to that of the parent material (the seating effect during initial contact for this type of compression measurement lowers the apparent stiffness of

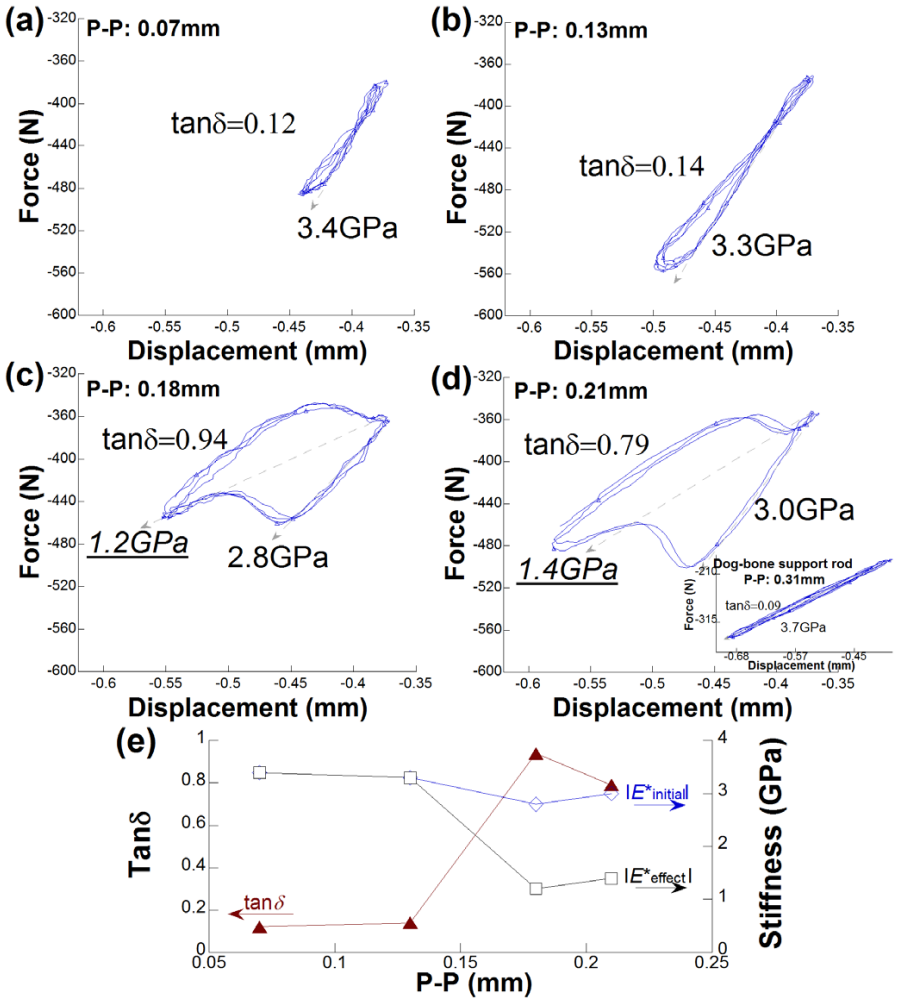

Figure 13. Force–displacement relationship of a PMMA axial damper module with two press-fit flat-ends PMMA columns ($L = 60$ mm; diameter $= 3.18$ mm) under 1 Hz compression tests with a pre-strain of 0.0055 for the press-fit columns. Insets show the force–displacement relationship of the dog-bone support rod (with the same pre-deformation) under 1 Hz compression tests with a peak-to-peak excursion (P–P) in displacement of 0.31 mm. Damping, initial stiffness, and effective stiffness of the module as a function of peak-to-peak excursion (P–P) in displacement are summarized in (e).

the module. The seating effect would also lead to a certain amount of deviation in terms of the onset strain of buckling for the press-fit columns during compression, and hence the mechanical behaviors between different modules even under the same strain). The force–displacement relationship of the dog-bone support rod without pre-strain is still in the linear range of viscoelasticity when spanning the peak-to-peak excursion (P–P) in displacement to about 0.85 mm (shown as the inset of figure 7(f)).

In addition to the effective stiffness, which is determined by the slope of the line passing through the initial loading point and splitting the Lissajous figure in half, the stiffness at the initial loading stage, which is determined by the slope of the tangent line of the initial loading portion (i.e., before the curve shows an apparent curvature) is also reported, and is called the initial stiffness.

3.4.2. Damper module with two press-fit flat-ends PMMA columns. Figure 8 shows the behaviors of a PMMA axial damper module with two press-fit 3.18 mm diameter 60 mm length flat-ends PMMA columns under 1 Hz compression tests without pre-strain. The inset of figure 8(a) shows the sketch of this module. The effective damping of the module increases with more press-fit columns provided these columns have buckled, and a maximum effective damping of about 0.21 was achieved in this module with appropriate AC amplitudes in deformation provided there is no pre-strain.

3.4.3. Damper module with four press-fit flat-ends PMMA columns. Figure 9 shows the behaviors of a PMMA axial damper module with four press-fit 3.18 mm diameter 60 mm length flat-ends PMMA columns under 1 Hz compression tests without pre-strain. The inset of figure 9(a) shows the

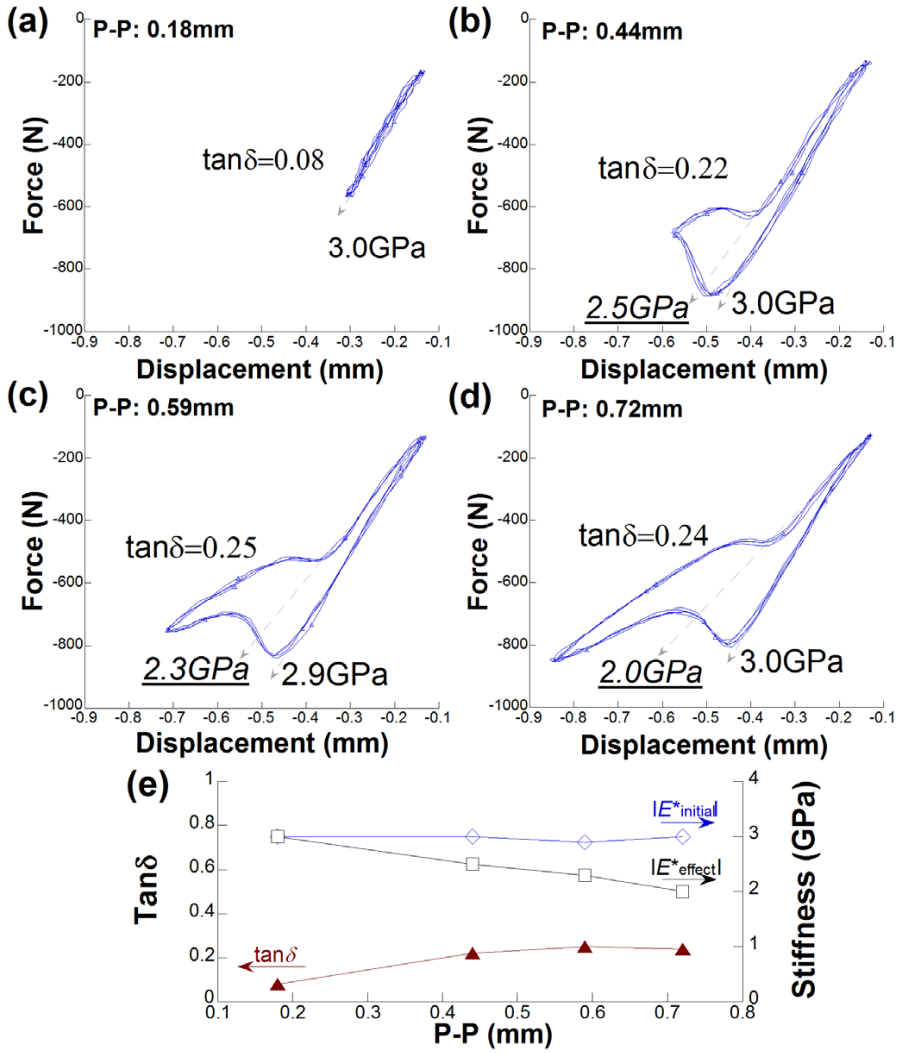

Figure 14. Force–displacement relationship of a PMMA axial damper module with four press-fit flat-ends PMMA columns ($L = 60$ mm; diameter $= 3.18$ mm) under 1 Hz compression tests with a pre-strain of 0.0013 for the press-fit columns. Damping, initial stiffness, and effective stiffness of the module as a function of peak-to-peak excursion (P–P) in displacement are summarized in (e).

sketch of this module. A maximum effective damping of about 0.21 was achieved in such a non-pre-strained module with appropriate AC amplitudes in deformation when the press-fit columns have post-buckled.

3.5. Effect of pre-strain on damping of press-fit flat-ends column in compression tests

Up to now, the properties have been studied without pre-strain. To attain higher effective damping, the properties of columns with pre-strain are investigated for 3.18 mm diameter 60 mm length press-contact flat-ends PMMA columns. As shown in figure 10, the linear portion of the Lissajous figure was reduced in length with an increasing pre-strain; only the segment corresponding to the post-buckling region (i.e., end-tilt buckling condition) remains. The effective damping gradually increases with increasing pre-strain, and can attain values even higher than 1 after the end condition is completely changed into edge contact. Furthermore, the effective stiffness remains negative when the end condition is completely changed.

3.6. Force–displacement relationship of a pre-strained damper module in compression tests

3.6.1. Damper module with two press-fit flat-ends PMMA columns. Figures 11–13 present the behaviors of the PMMA axial damper module with two press-fit 3.18 mm diameter 60 mm length PMMA columns with pre-strains of 0.0023, 0.0036 and 0.0055. The dog-bone support rods are still in the linear property range under the maximum strain amplitude applied (properties are shown as insets;

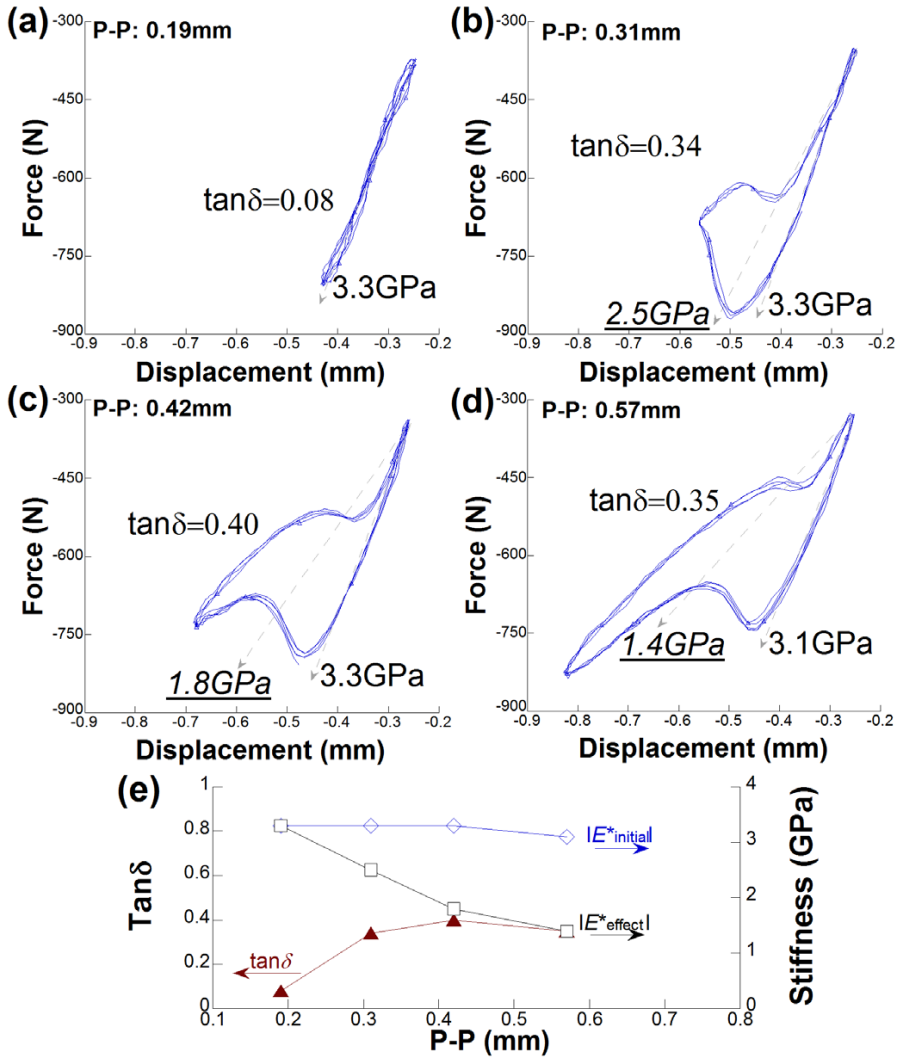

Figure 15. Force–displacement relationship of a PMMA axial damper module with four press-fit flat-ends PMMA columns ($L = 60$ mm; diameter $= 3.18$ mm) under 1 Hz compression tests with a pre-strain of 0.0034 for the press-fit columns. Damping, initial stiffness, and effective stiffness of the module as a function of peak-to-peak excursion (P–P) in displacement are summarized in (e).

damping is a little bit higher than that of the parent material, and is considered as the contribution from the friction inside the drilled holes). Damping, initial stiffness and effective stiffness of the module as a function of peak-to-peak excursion (P–P) in displacement are summarized in each figure (figures 11(e), 12(e) and 13(e)). The effective damping attains about 0.28 with a pre-strain of 0.0023, 0.32 with a pre-strain of 0.0036 and 0.94 with a pre-strain of 0.0055. The greatly enhanced damping when the pre-strain approaches 0.0055 is attributed to the onset of the change in the end condition from surface to edge contact. The stiffness of the module keeps decreasing with increasing pre-strain and AC amplitude in displacement. A maximum effective stiffness–damping product of approximately 1.1 GPa, and initial stiffness–damping product of approximately 2.6 GPa were achieved in this pre-strained module.

3.6.2. Damper module with four press-fit flat-ends PMMA columns. Figures 14–16 present the behaviors of the PMMA axial damper module with four press-fit 3.18 mm diameter 60 mm length PMMA columns with pre-strains of 0.0013, 0.0034 and 0.0054. Damping, initial stiffness and effective stiffness of the module as a function of peak-to-peak excursion (P–P) in displacement are summarized in each figure (figures 14(e), 15(e) and 16(e)). The effective damping attained values of about 0.25 with a pre-strain of 0.0013, 0.40 with a pre-strain of 0.0034 and 0.98 with a pre-strain of 0.0054, which is a significant improvement by more than a factor of fifteen over the intrinsic damping of PMMA. Moreover, the large damping occurs within the small strain glassy regime of PMMA, hence it is usable over a much wider range of temperature and frequency than polymer damping layers based on the high damping that occurs in

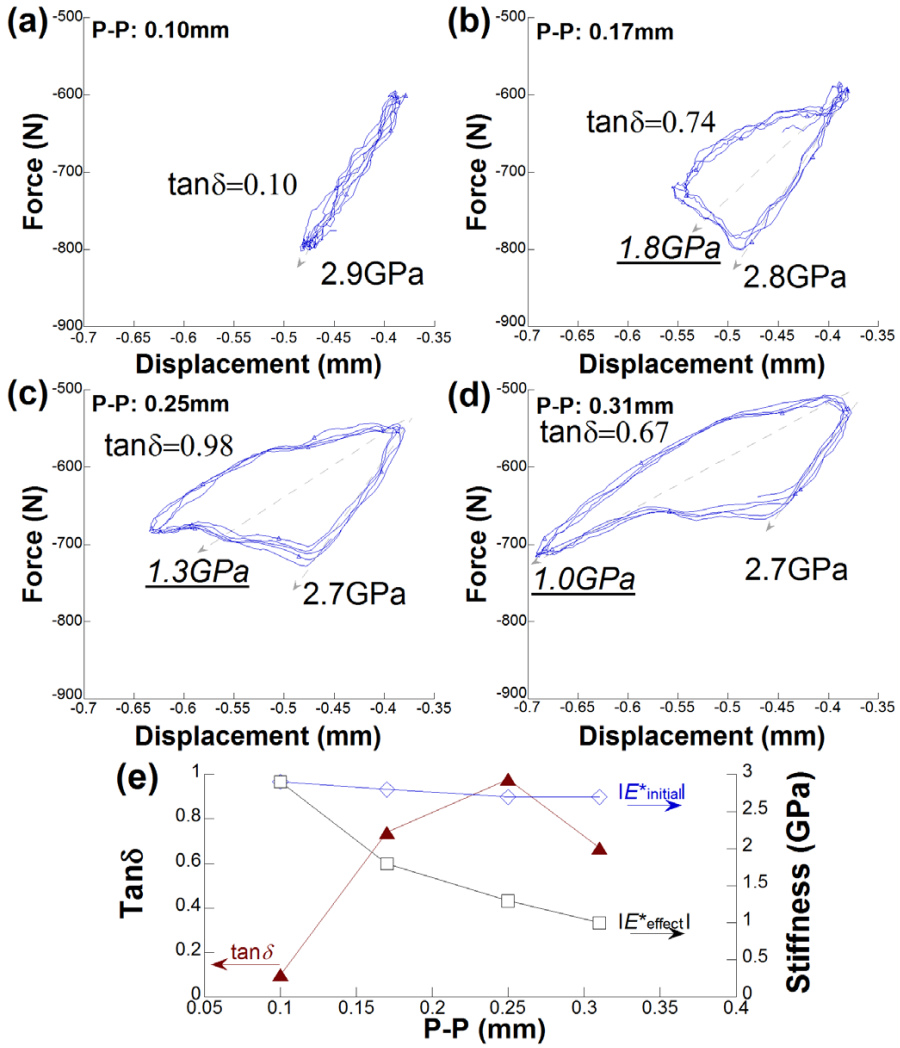

Figure 16. Force–displacement relationship of PMMA axial damper module with four press-fit flat-ends PMMA columns ($L = 60$ mm; diameter $= 3.18$ mm) under 1 Hz compression tests with a pre-strain of 0.0054 for the press-fit columns. Damping, initial stiffness, and effective stiffness of the module as a function of peak-to-peak excursion (P–P) in displacement are summarized in (e).

the leathery regime in the vicinity of the glass to rubber transition. A maximum effective stiffness–damping product of approximately 1.3 GPa, and initial stiffness–damping product of approximately 2.6 GPa were achieved in this pre-strained module. By contrast, polymer damping layers exhibit a maximum of about 0.6 GPa over a narrow range of temperature or frequency.

3.7. Comparison with other high-damping systems

A comparison with other high-damping systems is as follows. Negative stiffness systems can give rise to extremely high damping; prior lumped systems involving buckled tubes [5] or buckled spring systems [15] or snap-through strips in transverse bending are compliant, so they are not appropriate for a design that calls for high damping and high stiffness. Similarly, vibration isolation via compliant suspensions [16, 17] uses negative stiffness to reduce the overall isolator stiffness and so are directed to different design requirements. High stiffness and damping can also be obtained in composites [18]. Nevertheless the use of structural buckling of common materials as done in this study can, in some settings, obviate the necessity of special materials.

4. Conclusion

Negative stiffness and large hysteresis (i.e., high damping) can be achieved in the post-buckling regime of flat-ends columns in a compression test when the tilting of the ends goes from surface to edge contact. Given a fixed pre-strain, damping of the press-contact flat-ends column will first increase then decrease with increasing AC amplitude in

displacement. Smaller diameter to length ratios can yield higher damping when the column has post-buckled; damping progressively increases with increasing pre-strain, and can achieve values higher than 1 when the end condition has completed changed into edge contact. Stable axial damper modules composed of clamped and press-fit flat-ends PMMA columns have been designed, built and tested. The effective damping was enhanced by the post-buckling effect of the press-fit columns. Given appropriate pre-strain, the effective damping of the axial damper module can attain approximately 1, and the effective stiffness–damping product can achieve approximately 1.3 GPa, which is a considerable improvement for this figure of merit, which generally cannot exceed 0.6 GPa for currently used damping layers.

Acknowledgment

Support from DARPA is gratefully acknowledged.

References

[1] Lakes R S 2009 *Viscoelastic Materials* (Cambridge: Cambridge University Press) pp 208–9
[2] Capps R N and Beumel L L 1990 Dynamic mechanical testing, application of polymer development to constrained layer damping *Sound and Vibration Damping with Polymers* ed R D Corsaro and L H Sperling (Washington, DC: American Chemical Society)
[3] Cremer L, Heckl M A and Ungar E E 1988 *Structure Borne Sound* 2nd edn (Berlin: Springer)
[4] Lakes R S 2001 Extreme damping in composite materials with a negative stiffness phase *Phys. Rev. Lett.* **86** 2897–900
[5] Lakes R S 2001 Extreme damping in compliant composites with a negative stiffness phase *Phil. Mag. Lett.* **81** 95–100
[6] Jaglinski T, Stone D S, Kochmann D and Lakes R S 2007 Materials with viscoelastic stiffness greater than diamond *Science* **315** 620–2
[7] Dong L, Stone D S and Lakes R S 2011 Extreme anelastic responses in $Zn_{80}Al_{20}$ matrix composites materials containing $BaTiO_3$ inclusion *Scr. Mater.* **65** 288–91
[8] Bazant Z and Cedolin L 1991 *Stability of Structures* (Oxford: Oxford University Press)
[9] Rosakis P, Ruina A and Lakes R S 1993 Microbuckling instability in elastomeric cellular solids *J. Mater. Sci.* **28** 4667–72
[10] Lakes R S 2009 *Viscoelastic Materials* (Cambridge: Cambridge University Press) pp 59–61
[11] Decerf J O 1988 Interpretation of the mechanical damping behavior of glassy polycarbonate strained in the non-linear range of deformation below the yield point *Polymer* **29** 641–5
[12] Illes K H and Breuer H 1963 Molecular motions in polyethylene terephthalate *J. Colloid Sci.* **18** 1–31
[13] Lee T, Lakes R S and Lal A 2000 Resonant ultrasound spectroscopy for measurement of mechanical damping: comparison with broadband viscoelastic spectroscopy *Rev. Sci. Instrum.* **71** 2855–61
[14] Hibbeler R C 1991 *Mechanics of Materials* (New York: Macmillan) pp 631–41
[15] Wang Y C and Lakes R S 2004 Stable extremely-high-damping discrete viscoelastic systems due to negative stiffness elements *Appl. Phys. Lett.* **84** 4451–3
[16] Platus D L 1992 Negative-stiffness-mechanism vibration isolation systems *Proc. SPIE* **1619** 44–54
[17] Takeshi M, Takefumi T and Masaya T 2003 Vibration isolation system using negative stiffness *JSME Int. J. Ser.* C **46** 807–12
[18] Ludwigson M, Swan C C and Lakes R S 2002 Damping and stiffness of particulate SiC–InSn composite *J. Compos. Mater.* **36** 2245–54